Acta Pharmaceutica Sinica B 2024;14(4):1827−1844

Chinese Pharmaceutical Association
Institute of Materia Medica, Chinese Academy of Medical Sciences

Acta Pharmaceutica Sinica B

www.elsevier.com/locate/apsb
www.sciencedirect.com

ORIGINAL ARTICLE

A mix & act liposomes of phospholipase A2-phosphatidylserine for acute brain detoxification by blood−brain barrier selective-opening

Zinan Zhang[a,†], Wenbin Cao[a,†], Huanchun Xing[b], Shuai Guo[c], Lijuan Huang[a], Lin Wang[a], Xin Sui[a], Kui Lu[b], Yuan Luo[a], Yongan Wang[a,*], Jun Yang[a,*]

[a]*State Key Laboratory of Toxicology and Medical Countermeasures, Beijing Institutes of Pharmacology and Toxicology, Beijing 100850, China*
[b]*Tianjin University of Science and Technology, Tianjin 300222, China*
[c]*Hebei University of Science and Technology, Shijiazhuang 050018, China*

Received 19 August 2023; received in revised form 7 November 2023; accepted 8 November 2023

KEY WORDS

Liposomes;
Phospholipase A2;
Phosphoserine;
Blood−brain barrier;
Selectively open;
Mix & act

Abstract In the treatment of central nervous system disease, the blood−brain barrier (BBB) is a major obstruction to drug delivery that must be overcome. In this study, we propose a brain-targeted delivery strategy based on selective opening of the BBB. This strategy allows some simple bare nanoparticles to enter the brain when mixed with special opening material; however, the BBB still maintains the ability to completely block molecules from passing through. Based on the screening of BBB opening and matrix delivery materials, we determined that phospholipase A2-catalyzed 1-palmitoyl-2-oleoyl-*sn*-glycero-3-phosphoserine liposomes can efficiently carry drugs into the brain immediately. At an effective dose, this delivery system is safe, especially with its effect on the BBB being reversible. This mix & act delivery system has a simple structure and rapid preparation, making it a strong potential candidate for drug delivery across the BBB.

© 2024 The Authors. Published by Elsevier B.V. on behalf of Chinese Pharmaceutical Association and Institute of Materia Medica, Chinese Academy of Medical Sciences. This is an open access article under the CC BY-NC-ND license (http://creativecommons.org/licenses/by-nc-nd/4.0/).

*Corresponding authors.
E-mail addresses: yonganw@126.com (Yongan Wang), ajaway@126.com (Jun Yang).
[†]These authors made equal contributions to this work.
Peer review under the responsibility of Chinese Pharmaceutical Association and Institute of Materia Medica, Chinese Academy of Medical Sciences.

https://doi.org/10.1016/j.apsb.2023.11.015
2211-3835 © 2024 The Authors. Published by Elsevier B.V. on behalf of Chinese Pharmaceutical Association and Institute of Materia Medica, Chinese Academy of Medical Sciences. This is an open access article under the CC BY-NC-ND license (http://creativecommons.org/licenses/by-nc-nd/4.0/).

1. Introduction

Brain diseases seriously threaten human health, including chronic disorders (*e.g.*, brain cancers[1] and neurodegenerative diseases[2]), and acute conditions (*e.g.*, cerebral infarction[3] and poisoning[4]). The most important complication in the treatment of brain diseases is the lack of effective therapeutic drugs, primarily owing to the barrier function of the blood−brain barrier (BBB)[5]. Recently, brain-targeted delivery systems (BTDS) that deliver drugs into the brain have been widely reported[6,7]. The effectiveness of BTDS has often relied heavily on the surface modification of nanoparticles by linking these with targeted peptides[8], proteins[9], and aptamers[10]. Many problems surrounding the druggability, quality control, and industrialization of these strategies have been highlighted[11]. Opening the BBB to improve drug permeability into the brain is another strategy for drug brain administration[12]. Physical and chemical processes, such as ultrasound[13,14] and mannitol[15,16], have been applied to allow drugs to penetrate the brain. However, the problems surrounding safety regarding BBB integrity and non-selective molecular penetration restrict the application of this method. Owing to these disadvantages, almost no BTDS have reached clinical development or have the potential for industrialization.

Liposomes and lipid nanoparticles, utilized in mRNA vaccines, are rarely mature, stable, and industrialized nano-delivery systems, which have been consistently used until recently[17,18]. However, there are still few reported liposomes with both quality control and brain-targeted function. The traditional construction strategy of brain targeting liposomes was linking targeting accessory onto the surface of liposomes[19,20] as same as other BTDS; however, this strategy still could not overcome this difficulty for druggability due to the linking process. Nonetheless, the best strategy against this complication is to produce a liposome with an extremely simple structure that does not possess any chemical modifications, but can effectively transport drugs into the brain.

Herein, we generated a method to selectively open the BBB; this strategy allowed certain simple and bare nanoparticles to penetrate the brain while maintaining the BBB barrier function against other molecules or particles. Based on initial screening, a suitable combination of delivery material and BBB opening component was found; specifically, we developed a mix & act delivery system (DS) combined with phospholipase A2 (PLA2)[21] and liposomes with phosphatidylserine (PS). The PS in this system could effectively deliver drugs into the brain only when combined with several drops of PLA2 solution immediately, without any additional processing steps. Furthermore, brain detoxification pharmacology was conducted to quickly reflect and screen the cerebral delivery effect of this DS. Finally, an effective brain-targeted antidote was also produced using this DS, which resulted in a high-efficacy therapeutic.

2. Materials and methods

2.1. Cell lines and animals

bEnd.3, BV2, Neuro-2a, RAW264.7 cells were obtained from the cell bank of Chinese Academy of Science, rat astrocytes were obtained from Suncell Biotechnology Co., Ltd., (Wuhan, China). The cells were cultured in Dulbecco's modified Eagle media (DMEM, Gibco, New York, USA), supplemented with 10% fetal bovine serum (FBS, Gibco, Australia), penicillin (100 U/mL, Gibco, New York, USA) and streptomycin (100 mg/mL, Gibco, New York, USA). Cells were placed in an incubator at 37 ± 0.5 °C with 5% CO_2 and 90% relative humidity and passaged every 2−3 days.

All experiments were performed in accordance with the Regulations of the Experimental Animal Administration, issued by the State Committee of Science and Technology of the People's Republic of China (November 14, 1988), the ARRIVE Guidelines and the Guidelines for Care and Use of Laboratory Animals of the Beijing Institute of Pharmacology and Toxicology. And the experiments were approved by the Animal Ethics Committee of the Beijing Institute of Pharmacology and Toxicology (IACUC permit number: IACUC-DWZX-2023-P649). Sprague−Dawley (SD) rats (2 weeks old) were obtained from SPF Biotechnology Co., Ltd. (Beijing, China), Kunming mice (20 ± 2 g) and C57BL/6N (19 ± 2 g) mice were obtained from Beijing Vital River Laboratory Animal Technology Co., Ltd. (Beijing, China). Rodents had free access to sterilized food and distilled water and were maintained in stainless steel cages filled with hardwood chips in an air-conditioned room on a 12:12 h light/dark.

2.2. Preparation of the BTDS

BTDS was composed of a delivery nanoparticle and opening material. In construction of delivery nanoparticle, six types of phospholipid, including 1-palmitoyl-2-oleoyl-*sn*-glycero-3-phosphoserine (POPS, Avanti Polar Lipids, Inc. Alabaster, AL, USA), 1,2-dimyristoyl-*sn*-glycero-3-phospho-L-serine (DMPS, Ruitaibio, Beijing, China), 1,2-dipalmitoyl-*sn*-glycero-3-phospho-L-serine (DPPS, Ruitaibio, Beijing, China), 1,2-dipalmitoyl-*sn*-glycero-3-phosphocholine (DPPC, Tokyo Chemical Industry Co., Ltd., Tokyo, Japan), 1,2-dimyristoyl-*sn*-glycero-3-phosphocholine (DMPC, Tokyo Chemical Industry Co., Ltd., Tokyo, Japan), and 2-dipalmitoyl-*sn*-glycero-3-phosphoethanolamine (DPPE, Cordenpharma, Switzerland) were used for preparation of liposomes using the film-ultrasonic method. Briefly, the phospholipid of POPS, DPPC, DMPC was first dissolved in chloroform (DMPS, DPPS, DPPE were dissolved in a mixture of chloroform and methanol at a ratio of 3/2, *v*/*v*). A thin film was generated by rotary evaporation at 30 °C slowly and desiccated until completely dry. The antidote or fluorescent dye was dispersed in PBS solution, added to the dry lipid film and ultrasound. Then the liposome suspension was extruded through a 100 nm polycarbonate membrane (Avanti Polar Lipids, Inc. Alabaster, AL, USA) by a syringe extruder to obtain liposomes. Mesoporous silica nanoparticles (MSN) were synthesized by the classical stöbler method as mentioned in previous reports[22] with mesoporous structure that could adsorb an antidote or a fluorescent dye. After preparation of delivery nanoparticle, the opening material of LPS (0.1 mg/mL, MedChemExpress, Monmouth Junction, New Jersey, USA), VEGF (0.1 μg/mL, MedChemExpress, Monmouth Junction, New Jersey, USA), 5′-*N*-ethylcarboxamidoadenosine (NECA, 5 μg/mL, MedChemExpress, Monmouth Junction, New Jersey, USA), mannitol (9 mg/mL, Baxter, Shanghai, China), borneol (0.1 mg/mL, Aladdin, Shanghai, China), or PLA2 (0.5 U/mL) was adding to the delivery nanoparticle suspension, respectively, to construct BTDS. The final BTDS suspension was stored at 4 °C.

2.3. Characterization of liposomes

The hydrodynamic diameter, size distribution, and zeta-potential of liposomes were measured by dynamic light scattering (DLS,

Zetasizer Nano ZS90; Malvern Panalytical, Malvern, UK), and the morphology was assessed by transmission electron microscopy (TEM, HT7800, HITACHI, Japan).

2.4. Drug release profile

The release profile of HI6 was measured using the dialysis method. Briefly, 2 mL of HI6, POPS-HI6 or POPS-HI6-PLA2 was added in a dialysis bag and immersed in 500 mL phosphate buffer at 37 or 4 °C with gentle stirring. Samples were collected at predetermined times points (1, 3, 5, 10, 15, 20, 30, 40, 50, 60, 120, and 240 min), and then analyzed by high performance liquid chromatography (HPLC; Agilent technologies, USA) method with C18 reverse-phase column (SHISEDO, 250 mm × 4.6 mm, Japan), and mobile phase of 5 mmol/L sodium *n*-heptanesulfonate and 0.12% trifluoroacetic acid in acetonitrile (85/15, *v*/*v*). The injection volume and flow rate were 20 μL and 1.5 mL/min, respectively. The detection wavelength was 300 nm and the column temperature was 30 °C.

2.5. Cellular studies

2.5.1. Penetration studies using BBB models in vitro

Rat brain microvascular endothelial cells (BMECs) were separated and cultivated to establish BBB model *in vitro* as previous reports[10,23,24]. BMECs were plated on fibronectin-coated 0.4 μm pore size Transwell Plates (24 mm Transwell®, Beijing Labgic Technology Co., Ltd., Beijing, China), at a density of 1×10^5 cells per well, and continuous growth for 2 weeks to allow the BMECs to form a monolayer. The permeability assay performed after the 4 h leakage verification that the liquid levels in the top and bottom chambers of the Transwell remained constant throughout the 4 h incubation period.

To investigate the ability and the pathway of different BTDS to cross the BBB, 1 mL of fluorescein labeled BTDS (POPS 0.8 mg/mL, cy5 0.01 mg/mL, Xian Ruixi Biological Technology Co., Ltd., Xi'an, China, DIO 0.01 mg/mL, Xi'an Ruixi Biological Technology Co., Ltd., Xi'an, China, PLA2, NECA 5 μg/mL, VEGF 0.1 μg/mL, LPS 0.1 mg/mL, borneol 0.1 mg/mL, Mannitol 9 mg/mL, respectively) was then added to the upper chamber. And the culture media in lower chamber were replaced with 2 mL transparent HBSS (Servicebio, Wuhan, China) to reduce interference and then collected at 30 min. The temperature in 37 or 4 °C was adjusted according to the experimental design.

The fluorescein stored in the BMECs was measured when it was extracted from monolayer of the Transwell film, which was soaked in 2 mL of DMSO (Aladdin, Shanghai, China) and 1% Triton (1:1 *v*/*v*, Zsbio, Beijing, China), stirred for 10 min, and then stood at 4 °C for 3 h. Then the solution was collected, centrifuged at 13,000 rpm for 10 min (3−18 K, Sigma, Germany), and then measured the fluorescence intensity.

To investigate the effect of efflux on BTDS crossing the BBB, HBSS (2 mL) and POPS-FLU or POPS-FLU-PLA2 (1 mL) was added into the lower and upper chamber, respectively. The POPS-FLU or POPS-FLU-PLA2 (1 mL) in the upper chamber was removed and replaced with HBSS after 30 min, and then the Transwell model was incubated at 37 °C, 4 °C and EPI (PSC833), respectively. Finally, supernants were collected form the upper chamber and measured the absorption at 490 nm.

2.5.2. Cell PI staining

To explore the ingredient and dosage of BTDS acted with cells, PI staining method was applied for investigating the cell membrane integrity. Cells incubated with materials in different concentrations as follows: PLA2 (0.05, 0.1, 0.5, 1, and 2 U/mL), POPS (100, 200, 400, 800, and 1600 μg/mL), LPS 18:1 (5, 20, 100, 200, and 500 μg/mL), LPS 16:1 (5, 20, 100, 200, and 500 μg/mL), LPE (5, 20, 100, 200, and 500 μg/mL), LPC (5, 20, 100, 200, and 500 μg/mL), oleic acid (1 mg/mL) and palmitic acid (1 mg/mL). Besides, cells treated with different adding order, temperature, or PLA2 inhibitors (Varespladib 100 mol/L, anthranilic acid 50 mol/L) were proceed, and then imaged *via* LSCM (Dragonfly 200, Andor Technology PLC, UK) after stained with PI (50 μg/mL, MedChemExpress, Monmouth Junction, New Jersey, USA), DIO (50 μg/mL) and hoechst 33342 (Thermo Fisher Scientific, Oregon, USA).

For searching the effective components from the reaction between PLA2 and lipid, POPS (4 mg/mL) mixing with PLA2 (0.5 U/mL) at 37 °C for 1 h. The product of POPS and PLA2 was separated the supernatant and the pellet by centrifugal filter (10 KD, Merck Millipore, 30 min, 5000×*g*, 4 °C, Darmstadt, Germany), and then incubated with cells, respectively. Following that, PI staining was performed.

To investigate whether the opening effect of BTDS on cells was reversible, POPS (800 μg/mL) + PLA2 (0.5 U/mL) was incubated with cells for 10 min and replaced with fresh complete medium. The cells were stained with PI, DIO and Hoechst at predetermined times points (1, 2, 4, 8, 12, and 24 h), following the procedure described previously. The fluorescently labeled cells were then imaged *via* LSCM (Dragonfly 200, Andor Technology PLC, UK).

Different cells including BV2, Neuro-2a, RAW264.7 and rat astrocytes acted with BTDS were performed. POPS (800 μg/mL) + PLA2 (0.5 U/mL) were added to the cells for 10 min at 37 °C. The cells were stained with PI, DIO and Hoechst, then were imaged *via* LSCM (Dragonfly 200, Andor Technology PLC, UK).

2.5.3. Western blot for tight junction (TJ) proteins

The bEnd.3 cells were seeded into 6-well plates at a density of 1×10^5 cells per well and incubated under standard conditions for TJ generation. After 7 days of incubation, the cells were washed with PBS and incubated with fresh medium. The cells were then incubated with PBS, POPS (800 μg/mL), PLA2 (0.5 U/mL) or POPS (800 μg/mL) + PLA2 (0.5 U/mL) 30 min at 37 °C, respectively. Membrane proteins were collected from cells by the Mem-PER Plus Membrane Protein Extraction Kit (Cat No. 89842, Thermo Fisher Scientific, Oregon, USA). Sample of membrane proteins was loaded on 10% SDS PAGE then separated at 80 V for 3 h, transferred to the nitrocellulose paper and blocked with skimmed milk and incubated with anti-zo-1 (ab216880, abcam, USA) and anti-occludin (Cat No. ab222691, abcam, USA) antibody overnight. Subsequently, samples were washed with TBST and incubated with Goat Anti-Rabbit IgG-HRP (1/2000, *v*/*v*, Zsbio, Beijing, China) for 1 h. After reaction, samples were washed with TBST to remove the unreacted antibody and developed with ECL substrate and exposed to X-ray film. Anti-β-actin antibody was used as loading control.

2.5.4. In vitro cell viability study

Cell Counting Kit-8 (CCK-8, Vazyme Biotech, Nanjing, China) assay was used to evaluate the cell viability of POPS, PLA2 and POPS + PLA2 treated with bEnd.3 cells. The cells were seeded

into 96-well plates at 20,000 cells per well and cultured for 24 h to attach, and then incubated with POPS (3.125, 6.25, 12.5, 25.50, 100, 200, 400, and 800 μg/mL), PLA2 (0.0039, 0.0078, 0.0156, 0.0312, 0.0625, 0.125, 0.25, 0.5, and 1 U/mL), POPS (800 μg/mL) mixed with PLA2 (0.0039, 0.0078, 0.0156, 0.0312, 0.0625, 0.125, 0.25, 0.5, and 1 U/mL) and POPS (3.125, 6.25, 12.5, 25.50, 100, 200, 400, and 800 μg/mL) mixed with PLA2 (0.1 U/mL) for 30 min, respectively. Then, the cells were treated with cell counting kit for 2 h at 37 °C. Six replicates were performed in each case. The absorbance was measured at 450 nm using a microplate reader (Molecular Devices, California, USA).

2.5.5. *In vitro hemolysis test*

Different volumes of HI-6 (3 mg/mL), POPS (8 mg/mL), PLA2 (25 U/mL) and BTDS (HI6 3 mg/mL, POPS 8 mg/mL, PLA2 25 U/mL) were added to 1 mL of red blood cell suspension (*v/v* 2%) and the total liquid volume was adjusted to 2 mL (drugs was diluted by different multiples). 1 mL of saline was added to 1 mL of red blood cell suspension as a negative control, while 1 mL of distilled water was added as a positive control. Five independent duplicate samples were used for each of the above groups. Samples were incubated at 37 °C for 3 h before centrifugation (3000 rpm, 10 min, 3−18K, Sigma, Germany) and the OD value of the supernatant was determined at a wavelength of 545 nm. The hemolysis rate was calculated by Eq. (1):

$$\text{Hemolysis rate } (\%) = [(OD_{treatment} - OD_{positive})/(OD_{negative} - OD_{positive})] \times 100 \quad (1)$$

where $OD_{treatment}$ is the OD of sample in treatment group, $OD_{positive}$ is the mean value of the OD of the positive control group, $OD_{negative}$ is the mean value of the OD of the negative control group.

2.6. *In vivo studies*

2.6.1. *Fluorescein in brain*

The C57BL/6N mice were intravenously administered with free FLU (1 mg/kg), BTDS loaded with FLU (phospholipid 80 mg/kg, MSN 20 mg/kg, FLU 1 mg/kg), and free FLU (1 mg/kg) with opening material (PLA2 25 U/kg, NECA 0.1 mg/kg, VEGF 2 μg/kg, LPS 2 mg/kg, borneol 50 mg/kg, mannitol 2 g/kg), respectively. After 1 h of administration, mice brains were collected, homogenized, and centrifuged at 4 °C for 10 min (13,000 rpm, 3−18K, Sigma, Germany) to obtain the supernatants. The fluorescence intensity of the supernatants was measured with Ex 499 nm, Em 517 nm. At the same time, mice were treated with the same drugs only except the substitution of FLU with Cy3. Brain tissues were collected, cryosectioned and imaged using LSCM (Dragonfly 200, Andor Technology PLC, UK).

2.6.2. *Determination of the acetylcholinesterase reactivation rate (ARR)*

Kunming mice were randomly divided into groups including untreated non-poisoned controls (blank), untreated soman-poisoned (130 μg/kg soman, poisoned), soman-poisoned and treated with HI-6 (30 mg/kg) solution and several treatment groups. Component doses in the treatment groups were list as follows: phospholipid (80 mg/kg), HI-6 (30 mg/kg), PLA2 (250 U/kg), NECA (0.1 mg/kg), VEGF (2 μg/kg), LPS (2 mg/kg), borneol (50 mg/kg), mannitol (2 g/kg), Varespladib (50 mg/kg, MedChemExpress, Monmouth Junction, New Jersey, USA), diphyline (50 mg/kg, MedChemExpress, Monmouth Junction, New Jersey, USA), anthranilic acid (50 mg/kg, MedChemExpress, Monmouth Junction, New Jersey, USA), PSC833 (10 mg/kg, MedChemExpress, Monmouth Junction, New Jersey, USA), SCH58261 (5 mg/kg, MedChemExpress, Monmouth Junction, New Jersey, USA). Among them, borneol and mannitol were administered in the same way mentioned before, and the five inhibitors were injected intraperitoneally 1 h in advance. The other treatments were carried out simultaneously with the exposure with soman. Blood and brain samples were collected 10 min later. Brains were collected, homogenized, and centrifugated at 4 °C for 10 min, (13,000 rpm, 3−18K, Sigma, Germany) to obtain the supernatants for subsequent analyses. Twenty microliters of blood or tissue supernatant diluted 50-fold were added per well of an EIA/RIA plate (Costar 9018; Sigma−Aldrich, Durham, USA). Adrenocorticotrophic hormone (30 μL of a 1% solution) and PBS (30 μL of a 0.1 mol/L solution) were added to three wells each. After incubation for 30 min at 37 °C, 5,5-dithiobis-2-nitrobenzoic acid (200 μL of a 1% solution) was added to each well and the optical density (OD) was measured at the wavelength of 415 nm. The ARR was calculated using Eq. (2):

$$\text{ARR } (\%) = [(OD_{treatment} - OD_{poisoned})/(OD_{blank} - OD_{poisoned})] \times 100 \quad (2)$$

where $OD_{treatment}$ is the OD value of the treatment group samples, OD_{blank} is the average OD value of the blank group samples, $OD_{poisoned}$ is the average OD value of the poisoned group samples.

2.6.3. *Evaluation of the survival time of poisoned animals*

Kunming mice were poisoned with soman (640 μg/kg). Thereafter, animals were either kept untreated, or treated with HI-6 (30 mg/kg) solution, BTDS I (POPS 80 mg/kg, HI-6 30 mg/kg, PLA2 25 U/kg), BTDS II (POPS 80 mg/kg, HI-6 30 mg/kg, PLA2 50 U/kg). The survival time of mice was recorded.

2.6.4. *Histopathological analysis*

Kunming mice were divided into 4 groups: untreated soman-poisoned group, soman-poisoned + HI6 (30 mg/kg) group, soman-poisoned + BTDS (POPS 80 mg/kg, HI6 30 mg/kg, PLA2 250 U/kg) group. The brains of the mice were collected and fixed in glutaraldehyde (3%) for 48 h. After that, dehydration and embedding the brains to cut into 4 μm sections and stained with hematoxylin and eosin. The images were then acquired by a light microscope.

2.6.5. *Safety of the BTDS in vivo*

Kunming mice were divided into 10 groups administered with drugs as follow: PBS group, POPS (80 mg/kg) group, POPS (80 mg/kg) + PLA2 (2.5, 25, 250, and 500 U/kg) 4 groups, PLA2 (2.5, 25, 250, and 500 U/kg) 4 groups. The major organs and blood of mice were collected after administrated 1 h later. The tissue samples were subjected to histopathological analysis. Blood samples were tested for biochemical indicators.

3. Results and discussion

3.1. *Design, synthesis, and characterization of BTDS*

We proposed a DS that selectively opens the BBB. This DS was composed of a delivery nanoparticle and opening material that were used to produce effective cerebral drug delivery with an

ultra-simple structure (Fig. 1A); overall, these components indicate strong prospects for this DS in industrialization. Liposomes with PS or phosphatidylcholine (PC) were chosen as delivery nanoparticles for constructing lipid-based particles with a deformable and active surface. As a control, mesoporous silicon nanoparticles (MSNs) were chosen and synthesized as solid particles with an inert and stable surface. For opening materials, the traditional BBB opening materials lipopolysaccharide (LPS)[25], vascular endothelial growth factor (VEGF)[26], adenosine receptor agonist 5′-*N*-ethylcarboxamidoadenosine (NECA)[27], mannitol[28], and borneol[29] were selected. LPS serves as the control group for the evaluation of opening material performance in some reports[25], while mannitol is widely used in clinical treatment for reducing intracranial pressure[28]. Borneol is the most common opening material even applied as drugs sometimes[29]. NECA[27] and VEGF[26] have discovered and proven the BBB opening function recently (Supporting Information Table S1). Although there are few reports on the influence of PLA2 on the BBB[30–32], this enzyme was also investigated as an opening material in this study due to its potential to interfere with the membrane structure.

Liposomes with 1-palmitoyl-2-oleoyl-*sn*-glycero-3-phosphoserine (POPS), 1,2-dimyristoyl-*sn*-glycero-3-phospho-L-serine (DMPS), 1,2-dipalmitoyl-*sn*-glycero-3-phospho-L-serine (DPPS), 1,2-dipalmitoyl-*sn*-glycero-3-phosphocholine (DPPC), 1,2-dimyristoyl-*sn*-glycero-3-phosphocholine (DMPC), and 2-dipalmitoyl-*sn*-glycero-3-phosphoethanolamine (DPPE), 1-stearoyl-2-oleoyl-*sn*-glycero-3-phosphocholine (SOPC) were prepared using the same extrusion method, respectively; these particles had a globular morphology (Fig. 1B) with a uniform size <200 nm in diameter (Fig. 1C), except for DPPS liposomes. All liposomes possessed a negative surface charge (Fig. 1D), which improved the stability of the suspension of nanoparticles. MSNs were synthesized using the classical stöbler method[22], with a uniform size of 100 nm in a globular shape and a mesoporous structure for adsorbing drugs (Fig. 1B).

After mixing with the opening material, the liposome may undergo small changes. LPS, NECA, mannitol, borneol and VEGF had no reported reaction with the phospholipid. Only PLA2 could catalyze the *sn*-2 cleavage of phospholipids. The liposome with POPS became denser when combined with PLA2, as shown in the corresponding TEM images (Fig. 1E and F); additionally, when combined with PLA2, the releasing speed of the POPS liposome was further accelerated by the liposome surface reaction with the enzyme even at 4 °C (Fig. 1G), lower than the phase inversion temperature (PIT) of POPS. But the releasing speed of POPS liposomes was lower than that in 37 °C, due to the inhibition of enzyme activity and nanoparticles in solid state without stretching (Supporting Information Fig. S1).

3.2. *Exploration of enlarge production*

Based on the mix & act BTDS strategy, no chemical reaction was required during the entire preparation process; this avoided extra coproduct production, the need for complex purification and separation, and excessive use of organic solvents. Liposomes of POPS were easily prepared using technology with stable high quality and yield such as syringe extrusion (Supporting Information Fig. S2A), high-pressure extrusion (Fig. S2B), and microfluidics methods (Fig. S2C) explored in this study. All

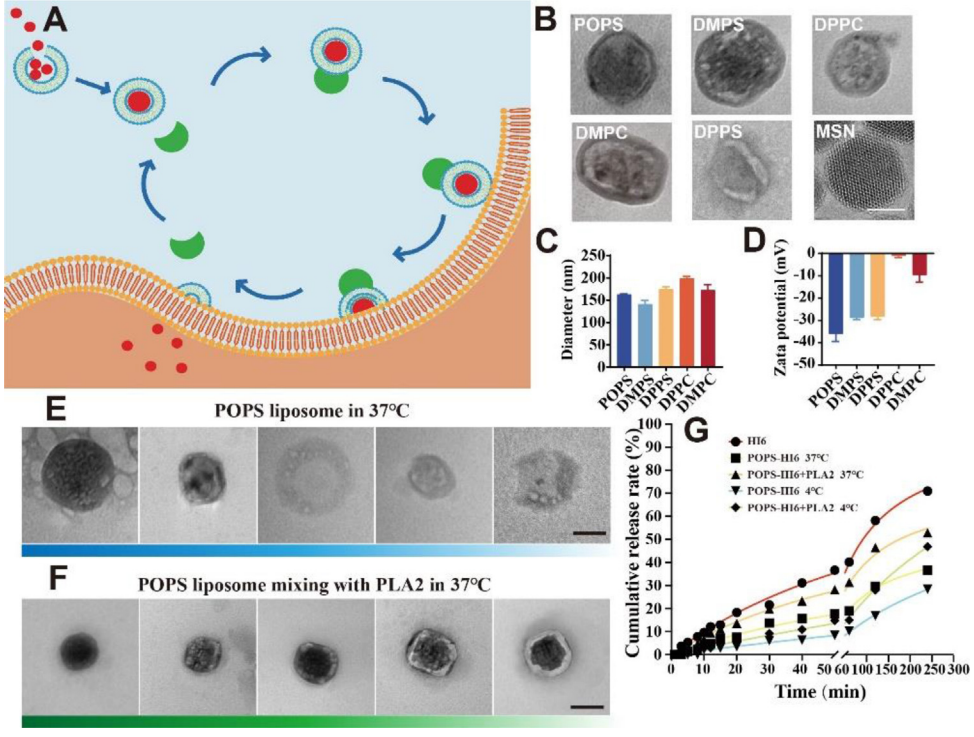

Figure 1 Characterization of Liposomes. (A) Schematic illustration of nanoparticles working in conjunction with opening materials to penetrate the brain. (B) Transmission electron microscopy (TEM) images of POPS-, DMPS-, DPPS-, DPPC- and DMPC-based nanoparticles; MSN. Scale bar = 50 nm. (C) Size of the different nanoparticles characterized by dynamic light scattering. Data are presented as mean ± SD (n = 3). (D) Zeta potential of the different nanoparticles. Data are presented as mean ± SD (n = 3). (E) The stability of POPS liposomes at 37 °C. Scale bar = 50 nm. (F) The stability of POPS liposomes combined with PLA2 at 37 °C. Scale bar = 50 nm. (G) Cumulative drug release rate of the different nanoparticle BTDS combined with PLA2 at different temperatures.

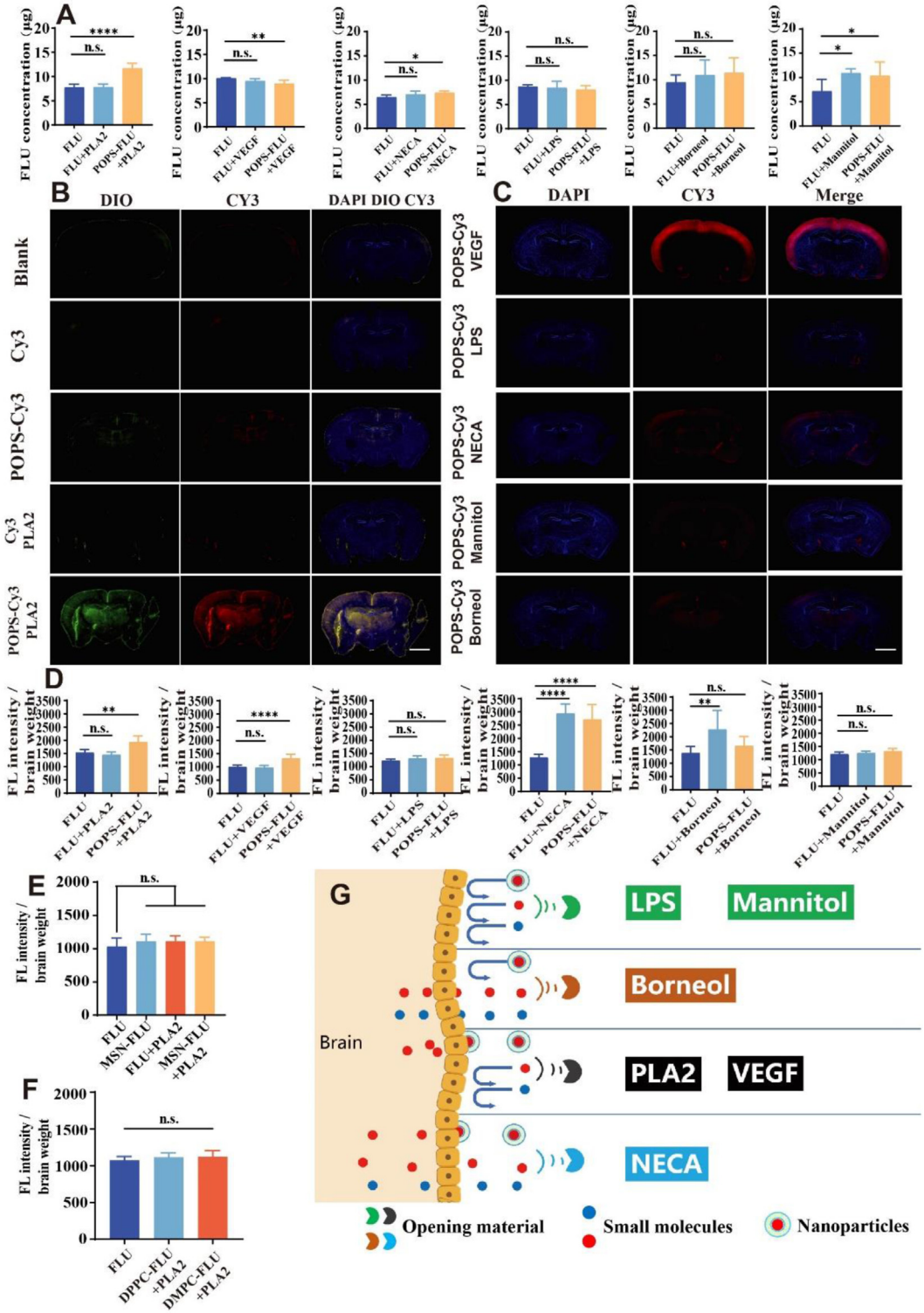

Figure 2 Brain target effect evaluation *in vitro* and *in vivo*. (A) The quality of fluorescein that penetrated into the lower chamber of the Transwell systems treated with different BTDS. Data are presented as mean ± SD ($n = 6$). (B,C) Fluorescence images of brain sections from mice treated with Cy3 or POPS-Cy3 in the presence or absence of higher levels of (B) PLA2, (C) VEGF, LPS, NECA, mannitol, and borneol. Scale bar = 200 μm. (D−F) The fluorescence intensity (FI) of dye delivered into the brain of mice treated with different (D) opening materials, (E) MSN, and (F) phosphatidylcholine. Data are presented as mean ± SD ($n = 6$). (G) Schematic representation of the varied BBB penetration activity following treatment with different combinations of nanoparticles and opening materials based on evaluation of fluorescent content in brain. *$P < 0.05$; **$P < 0.01$; ***$P < 0.001$, ****$P < 0.0001$ *vs.* indicated. n.s., not significant.

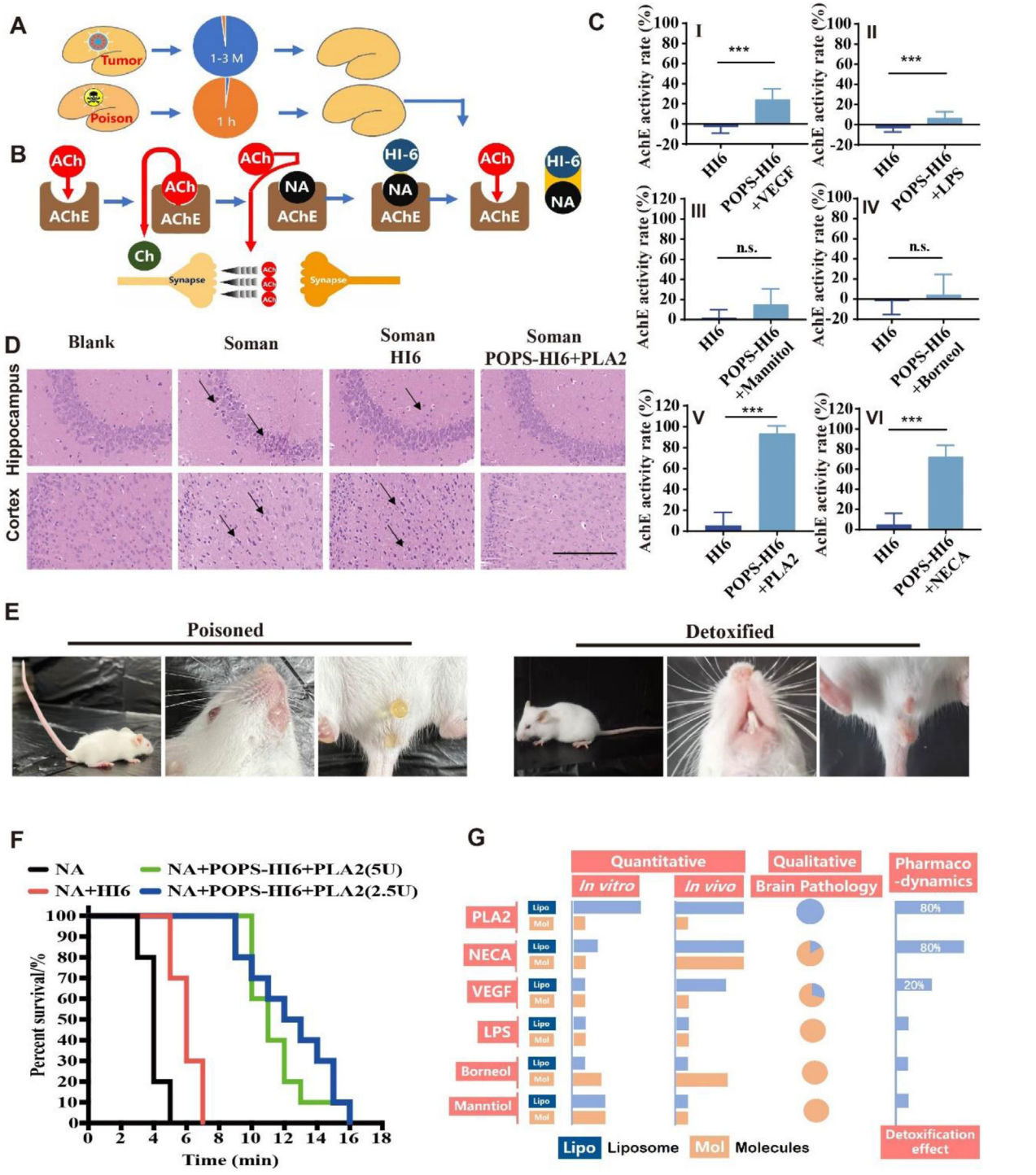

Figure 3 The detoxification potential of HI-6-loaded BTDS. (A) Comparison of disease treatment time between chronic disease and acute poisoning in brain. (B) Schematic illustration of poisoning and the corresponding reactivation process of the cholinergic system. (C) Mouse brain AChE reactivation rate when treated with different BTDS loaded with HI-6 after being poisoned with the soman. Data are presented as mean ± SD ($n = 12$). (D) Images showing hematoxylin and eosin (H&E)-stained brain sections from the groups treated with antidotes. Scale bar = 200 μm. (E) Images showing the symptoms of stiffness of the tail, salivation, and incontinence before and after detoxification treatment. (F) The survival time of mice poisoned with soman (640 μg/kg) and treated with POPS liposome antidotes. (G) Summary and comparison of different brain targeting systems and the pharmacodynamics evaluation *in vitro* and *in vivo*. ***$P < 0.001$ *vs.* indicated. n.s., not significant.

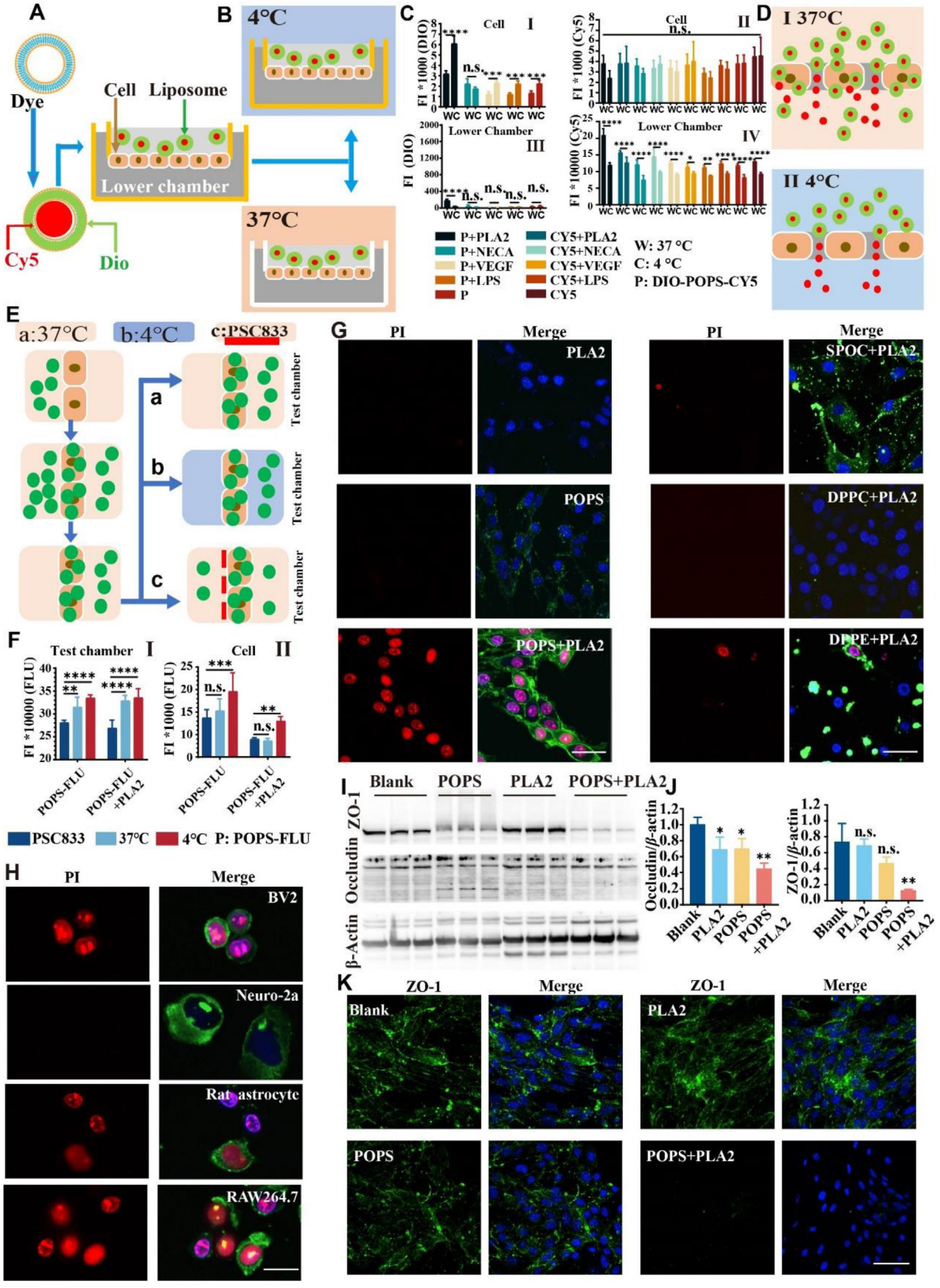

Figure 4 The mechanism of brain targeting effect evaluation *in vitro*. (A) Schematic illustration of red and green fluorescence-labeled POPS liposomes. (B) The processing flow scheme of BTDS penetrating the Transwell system across different temperature treatments. (C) The FI of fluorescence dye in the (I, II) cell layer and (III, IV) lower chamber. Data are presented as mean ± SD ($n = 6$). (D) Schematic representation of the process of liposomes penetrating the cell layer in Transwell model. (E) The processing flow scheme of BTDS efflux treated at (a) 37 °C, (b)

liposomes prepared by different methods maintained the same morphology (Fig. S2D) and surface charge (Fig. S2E). The widely used microfluidic method, which is used in mRNA vaccine production, could also be applied for POPS liposome preparation, with the smallest size of product than that prepared from other methods (Fig. S2F). Using a high-pressure extruder, 20 mL of sample was produced in one round, which was 20 times greater than that prepared by syringe extrusion method (1 mL) used in this study. Nonetheless, nearly 50 mL of POPS liposomes could be prepared by the microfluidic method (Fig. S2G). This BTDS using POPS was a rare DS that had potential for industrialization.

3.3. *Evaluation of targeting the central nervous system*

The central targeting properties of these BTDS were investigated *in vitro* and *in vivo*. As shown in Fig. 2A, these liposomes with POPS could only transport FLU across the barrier with the assistance of PLA2 or NECA; this was proven by monitoring the FLU levels in the lower chamber of a Transwell system *in vitro*[10,23,24]. For the solid nanoparticles with MSNs, none of the opening materials used could open the BBB to allow these nanoparticles into the lower chamber (Supporting Information Fig. S3). Corresponding results were also obtained *in vivo*. Only POPS liposomes with the assistance of PLA2 could effectively transport the loading content into the brain, which was preliminarily shown by the brain fluorescence pathology (Fig. 2B and C). The NECA administration group showed slight red Cy3 fluorescence in the brain pathology evaluation. It was interesting that VEGF can only confer the transport of POPS liposomes to the cortex of the outer edge of the brain (Fig. 2C). Accurately measuring the fluorescent content that was transported into the brain (Fig. 2D) revealed that borneol completely opened the BBB, allowing all exogenetic molecules to penetrate into the brain; however, the liposome did not enter the brain under these conditions. All the POPS liposome and exogenetic molecules could cross the BBB into the brain with the help of NECA. Additionally, POPS liposomes combined with PLA2 could cross into the brain at significant levels, whereas the exogenetic molecules remain blocked outside of the brain. VEGF also possessed this same function, but with a lower efficacy than PLA2. No obvious fluorescence was observed in the brain in the groups treated with POPS liposomes mixing with LPS and mannitol (Fig. 2D), MSNs combined with all opening materials (Fig. 2E, and Supporting Information Fig. S4) and PLA2 incorporated with other liposomes (Fig. 2F). In brief, opening materials led to different penetration effects (Fig. 2G); only the BTDS composed of POPS liposome mixed with PLA2 could effectively transport drugs into the brain while maintaining the BBB function against exogenetic molecules.

3.4. *The acute brain detoxification potential of HI-6-loaded BTDS against NA*

Pharmacodynamic evaluation is the accepted, accurate, and final method used for the evaluation of brain-targeted drugs. In traditional reports, most brain-targeted drugs have been focused on cancers or neurodegenerative diseases[33]. The pharmacodynamic evaluation of these chronic diseases requires for more than 1−3 months form establishing suitable animal models to evaluate its efficacy[34,35]; ultimately, this method is not suitable for fast, large-scale BTDS screening and innovation. Nonetheless, there has been a strong demand for BTDS in emergency brain poisoning treatment (Fig. 3A). Organophosphorus inhibit the cerebral enzyme acetylcholinesterase (AChE) and cause immediate death; therefore, to treat this poisoning, the corresponding antidote needs to pass across the BBB quickly. Unfortunately, reactivator antidotes, such as HI-6 (asoxime chloride), which detach the organophosphorus from AChE to recover the cholinergic system[36], cannot cross into the brain to confer this function[37]. The ideal BTDS should carry the corresponding antidote into the brain to reactivate AChE, leading to detoxification (Fig. 3B). This therapeutic effect could be quantitatively analyzed by assessing enzymatic activity over the entire detoxification process (1 h) to determine the final efficiency of different BTDS[38]. Therefore, in this study, BTDS were utilized in brain detoxification against organophosphorus; this was conducted to not only quickly verify the efficacy of these BTDS, but also to allow efficient implementation against terrorist threats of the chemical weapon, organophosphorus[39].

For pharmacodynamic evaluation of brain-targeted antidote, the organophosphorus soman was utilized for brain poisoning. The reactivator HI-6 was loaded into POPS liposomes (POPS-HI-6). In the resultant analysis of the brain AChE activity rate (AAR), the AAR of VEGF-treated groups (Fig. 3C and I) was nearly 20 times greater than that of the HI-6 solution-treated group; this was consistent with prior results, presented in Fig. 2C and D. The AAR from LPS-treated groups may be caused by the tiny free HI-6 being able to penetrate into the brain to detoxify inhibited enzyme (Fig. 3C II). It's worth noting that the negligible amount of penetrated drugs such as transporting into brain with the help of LPS could not be detected and recognized by the traditional methods (Fig. 2) due to its low content. The groups treated with the commonly used cerebral opening materials borneol and mannitol showed no brain AAR (Fig. 3C III and IV). In contrast, the combination of NECA and PLA2 with POPS-HI-6 demonstrated a remarkable effect in brain AAR (Fig. 3C V and VI), Specifically, this group reached nearly 80% reactivation, which was 4, 10, and 30−40 times higher than that of VEGF, LPS, and bare HI-6 solution (AAR 4%), respectively; this AAR was far beyond those achieved in prior studies[10,22]. This data revealed that the combination of PLA2 and POPS liposomes provided effective delivery of drugs into the brain to effectively treat cerebral disease.

The further beneficial treatment effects provided by this BTDS were evaluated sequentially. Cell apoptosis and large edema foci were detected in the cerebral cortex and hippocampal CA2 region of the poisoned and HI-6-treated groups. After treatment with POPS-HI-6-PLA2, most of the pyramidal cells in the hippocampus remained morphologically normal and compact in arrangement (Fig. 3D). Regarding behavior, the poisoned mice

4 °C, and (c) EPI (PSC833). (F) FI of dye efflux (I) back into the test chamber and (II) stored in the cell layer. Data are presented as mean ± SD ($n = 3$). (G) PI staining for cell membrane permeability when cells treated with different liposomes combined with PLA2. Scale bar = 50 μm. (H) PI staining for cell membrane permeability of different cells treated with POPS combined with PLA2. Scale bar = 20 μm. (I) Western blot of occludin and ZO-1 protein expression from cells treated with POPS combined with PLA2. (J) Densitometric analysis of the Western blot data. Data are presented as mean ± SD ($n = 3$). (K) Immunofluorescence images of ZO-1 in cells treated with POPS combined with PLA2. Scale bar = 50 μm. *$P < 0.05$; **$P < 0.01$; ***$P < 0.001$, ****$P < 0.0001$ *vs.* indicated. n.s., not significant.

developed a series of symptoms: salivation, incontinence, stiffness of the tail (Fig. 3E) and convulsion (Supporting Information Vedio S1). While the mice treated with POPS-HI-6-PLA2 remained stable and silent. Even with poisoning at three times higher than the lethal dose, the average survival time extended from 4 to 13 min after administration of POPS-HI-6-PLA2 (Fig. 3F); this additional 9 min gained may provide a pivotal chance for subsequent comprehensive treatment, including oxygen supplementation, anticonvulsants, and continuous AChE reactivation. Overall, this data revealed the protective effect of POPS-HI-6-PLA2 in the context of soman-induced brain injury.

Supporting video related to this article can be found at https://doi.org/10.1016/j.apsb.2023.11.015.

Compared with the brain targeting data (Fig. 2A−D) and the resultant therapeutic effect of drugs implementing this BTDS (Fig. 3C), it was interesting that the targeting results obtained by the different methods were sometimes inconsistent (Fig. 3G), due to individual differences alongside the accuracy and universality of the test method; this was specifically observed in the differing results obtained *in vitro* and *in vivo* in the VEGF, NECA and borneol treated group. Crucially, only the data produced by the pharmacodynamic results of brain detoxification can truly reflect the therapeutic effect of the drug's targeting system (Fig. 3C). Therefore, it is strongly suggested that the pharmacodynamic evaluation of central poisoning treatment could be used as the core verification method to determine the central targeting of DS under the provided conditions.

3.5. *The mechanism of targeting the central nervous system*

The mechanisms underlying the selective BBB opening strategy were investigated. The initial targeting site was first investigated using a Transwell cell barrier model *in vitro*. The POPS liposome was stained with DIO (green) in the phospholipid membrane and loaded with fluorescein Cy5 (red) for characterization of the matrix and of the cargo penetration properties, respectively (Fig. 4A). The Transwell model was also tested at 4 °C when the cell uptake inhibited to investigate inter- and intra-cellular penetration by measuring the fluorescence observed both in the lower chamber and cell layer (Fig. 4B). The DIO fluorescence of bEnd.3 cells treated with PLA2 at 4 °C was higher than any other treated groups, including at 37 °C; this proved that the POPS liposomes could penetrate the barrier *via* tight junctions (TJs) in an intercellular manner, even with cell uptake inhibition (Fig. 4C I). Alternatively, no significant difference in Cy5 expression was observed between any cells; this indicated that most hydrophilic molecules that penetrated into cells leaked out from the cell layer into the lower chamber without being stored (Fig. 4C II). In the lower chamber, the group treated with POPS liposomes at 37 °C showed the highest DIO (Fig. 4C III) and Cy5 (Fig. 4C IV) fluorescence. Additionally, part of the POPS liposome could maintain its particle morphology, even when passing into the cell at 37 °C in all groups in the Transwell assays; specifically, this was proven (Fig. 4C III) and illustrated (Fig. 4D I) by the observation of penetrative DIO across all groups. The liposomes could also penetrate intercellularly *via* TJs; however, phospholipid of POPS entrapment would occur in the TJs, and only the loaded hydrophilic content could continue through (Fig. 4D II).

In the improved Transwell system for efflux effect investigation (Fig. 4E), the fluorescein in the test chamber significantly decreased after treatment with efflux pump inhibitor (EPI) PSC833, whereas the fluorescein expression in the low temperature-treated and untreated groups remained the same, whether or not PLA2 was added (Fig. 4F I). Meanwhile, EPI did not increase the fluorescein storage in bEnd.3 cells (Fig. 4F II). The central efflux could be effectively inhibited by EPI, preventing the loss of existing cerebral molecules. Therefore, drug delivery could be enhanced by inhibiting the efflux pump to some degree; however, BTDS of POPS-PLA2 did not interfere with the barrier efflux process.

More detailed investigation of the combination of PLA2 and POPS liposomes was conducted to establish the specific potential targets at the cell membrane and TJs. The TEM images about TJs before and after POPS-PLA2 treated proved the BBB opening directly (Supporting Information Fig. S5). Furthermore, propidium iodide (PI) staining does not only reflect the occurrence of cell apoptosis but is also a method used to assess the permeability of the cell membrane[40]. The cell nuclei were only stained with PI when treated with POPS combined with PLA2 (Fig. 4G), which resulted in the penetration of PI through the membrane. However, no staining was achieved when treating with POPS or PLA2 separately. The other liposome materials, such as DPPC, DPPE, and SOPC, combined with PLA2 showed no observable PI staining (Fig. 4G). Alongside the bEnd.3 cells, other cell types were also stained with PI when treated with the combination of POPS and PLA2, except for Neuro-2a cells (Fig. 4H). However, the cause for this exception in Neuro-2a cells is currently unknown and requires further investigation. Additionally, the potential proteins affected in TJs were investigated by Western blot analysis (Fig. 4I and J) and immunofluorescence (Fig. 4K). After being treated with POPS-PLA2, the expression of the TJ proteins ZO-1 and occludin significantly decreased in TJs; this caused an increase in TJ permeability and led to some nanoparticle transport into the brain. And the combination of other opening materials with POPS did not effectively reduce the expression of ZO-1 protein as show in immunofluorescence (Supporting Information Fig. S6). Overall, these results revealed that only the combined treatment of POPS and PLA2 affected the permeability of the cell membrane, the expression of ZO-1 and occludin in TJs, and promoted nanoparticle transport across the cell barrier, as illustrated in Fig. 4D.

Pharmacodynamic evaluation of brain detoxification was applied to more accurately indicate the target pathway. After mixing with PSC833, the AAR from mice treated with the nanoantidote of POPS-HI-6-PLA2 was significantly increased (Fig. 5A), which was consistent with the Transwell results (Fig. 4F). However, treatment with *N*-(*p*-amylcinnamoyl) anthranilic acid (ACA; a PLA2 inhibitor) (Fig. 5B) and diphylline (adenosine receptor inhibitor) (Fig. 5C) showed a remarkable decrease in this detoxification effect; this indicated that the PLA2 enzyme activity and membrane permeability have an important impact on brain delivery properties. It's worth noting that the PLA2 inhibitor was specific. The PLA2 from bee venom was applied in our study, which was different from the exogenous group II secretory PLA2 producing during inflammation or as an endogenous snake venom. The inhibitor varespladib, selectively inhibiting the latter ones[41], had no influence on AAR (Fig. 5C) when mixing with PLA2-POPS; this indicated that different types of enzymes were independent with each other, and inhibiting one PLA2 enzyme didn't affect other types of enzymes. Without PLA2 addition, no inhibitors showed any effect on increasing or decreasing the ARR (SCH58261, adenosine A2A receptor

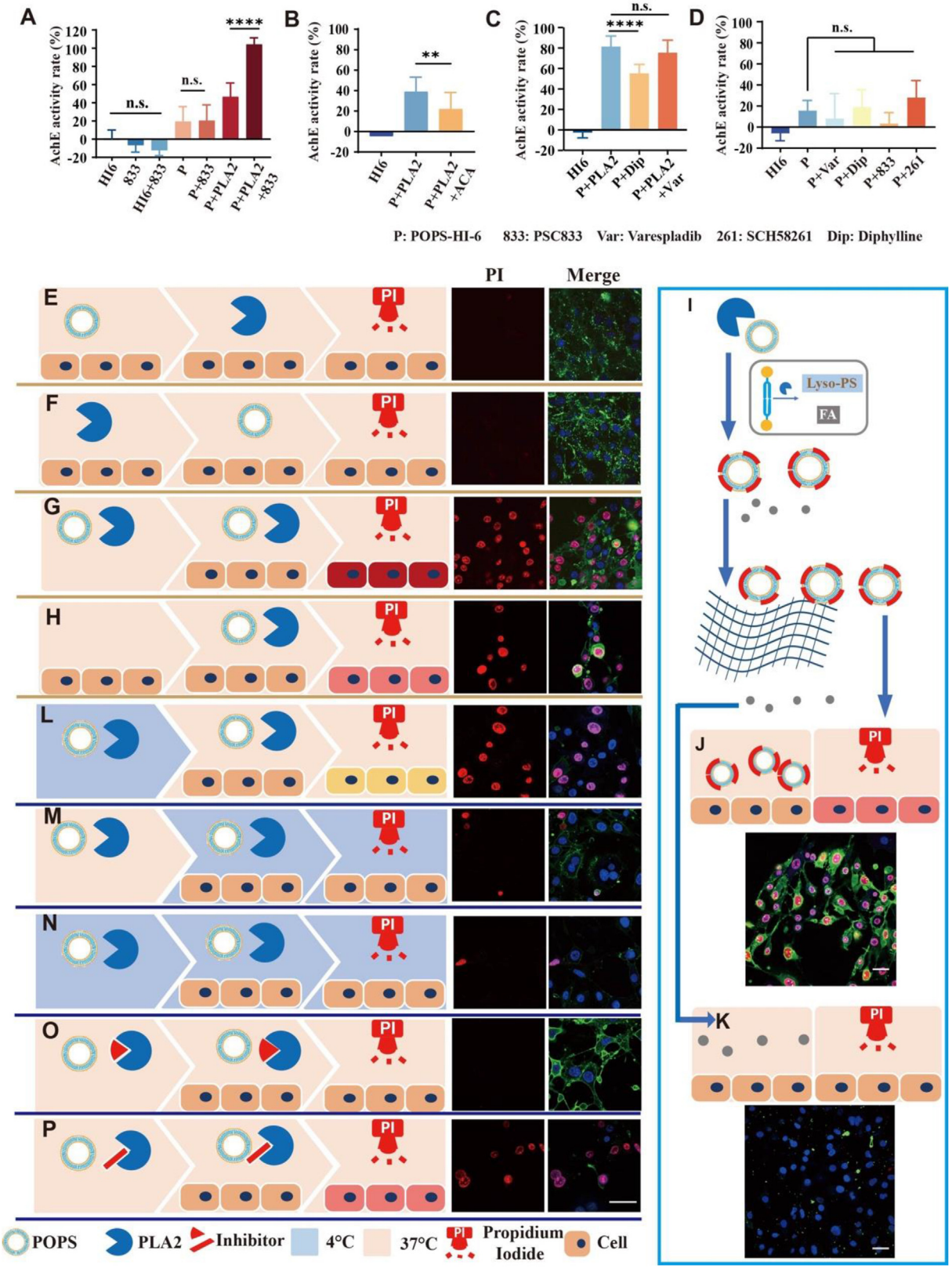

Figure 5 The investigation of factors influencing the interaction between POPS and PLA2. (A−C) The brain ARR when treated with PSC833, PLA2 inhibitor ACA, adenosine receptor inhibitor diphylline, and PLA2 inhibitor varespladib combined with PLA2. Data are presented as mean ± SD (n = 10). (D) The brain ARR when treated with different inhibitors but without PLA2. Data are presented as mean ± SD (n = 10). (E−P) Schematic diagrams of different treatment methods of PLA2 and POPS interaction with the cell (left) and fluorescent images of PI staining (right): (E−H) different mixing orders of PLA2 and POPS, (I−K) reaction components, (L−N) incubation temperatures, and (O−P) PLA2 inhibitors. Scale bar = 50 μm. $^{**}P < 0.01$; $^{****}P < 0.0001$ *vs.* indicated. n.s., not significant.

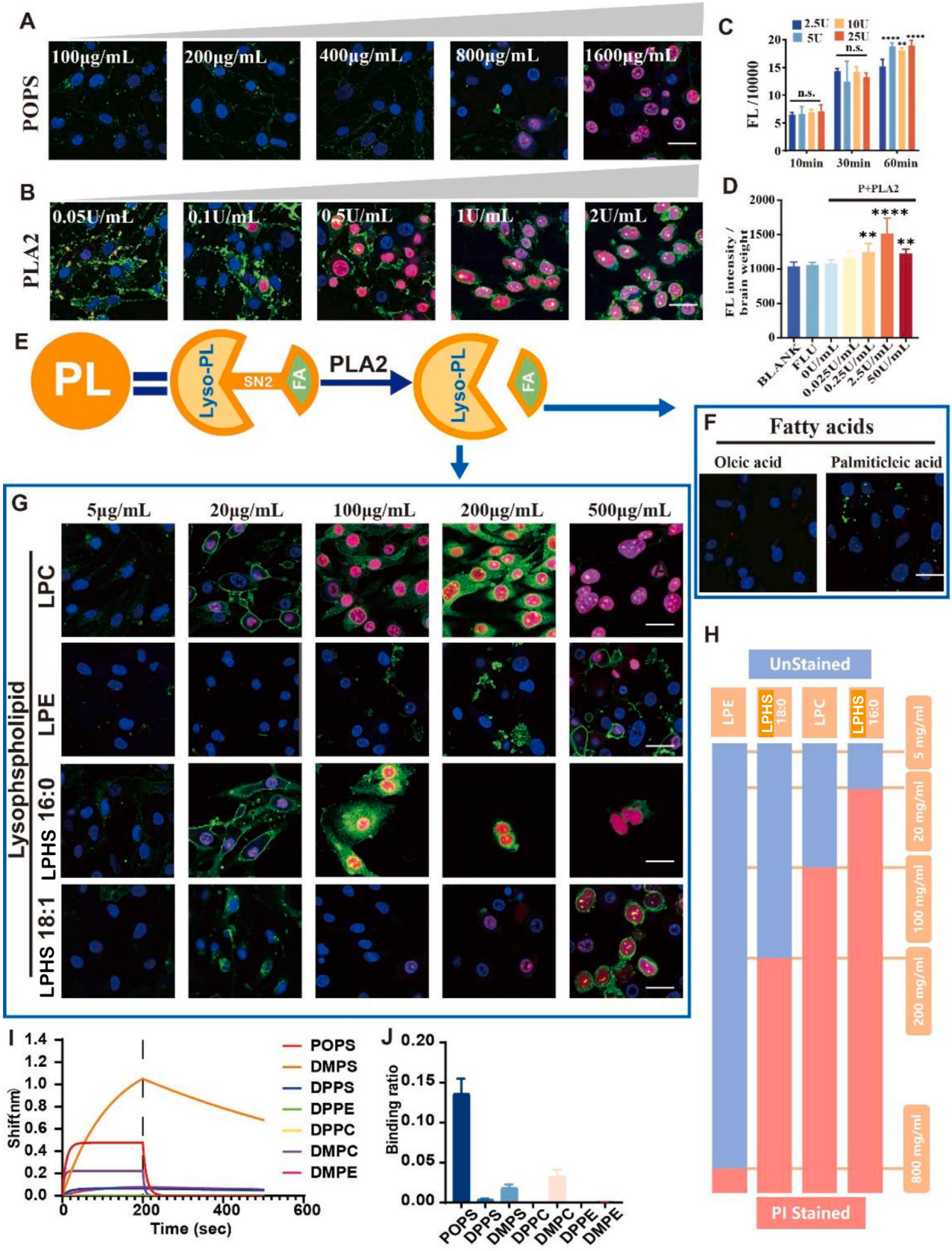

Figure 6 The brain targeting active product generated by PLA2 catalytic reacted with POPS. (A, B) Fluorescent images of PI staining with different concentrations of POPS and PLA2. (A) 800 μg/mL POPS, 0.05−2 U/mL PLA2. Scale bar = 200 μm. (B) 2 U/mL PLA2, 100−1600 μg/mL POPS. (C) The FI of dye carried by POPS combined with PLA2 penetrating the cell layer of the Transwell model. Data are

antagonist) (Fig. 5D); this effect further proved that PLA2 was key for the BTDS.

The binding order between cells, POPS, and PLA2 should be verified. The effects of adding components in a special order was illustrated in Fig. 5E−H. If the cells were initially treated with either POPS (Fig. 5E) or PLA2 (Fig. 5F) individually for 10 min, and then the other component was added after removing the former, the PI could not penetrate into the cell to stain the nucleus. When POPS was combined with PLA2 for 10 min and this mixture was added into the cell (Fig. 5G), the PI staining was distinctly greater than that when POPS and PLA2 were added to the cells simultaneously (Fig. 5H). These results demonstrated that POPS or PLA2 alone did not interact effectively with the cells. Specifically, PLA2 initially reacted with POPS to modify the POPS liposome surface to enable its penetration ability; this combination could then interact with corresponding cells. To further proving this, the interaction of PLA2 with POPS was characterized using ultrafiltration membrane technology (Fig. 5I). After PLA2 reacted with POPS for 10 min, the reacted liposome nanoparticles and reaction liquid, which may contain the molecules formed by the PLA2-catalyzed cleavage of POPS, were separated by ultrafiltration. These separated two products were added into cells for PI staining, respectively. The cells maintain the same state without PI-stained when mixing with the reaction liquid (Fig. 5K), but stained when treated with the PLA2-reacted liposome nanoparticles (Fig. 5J); this further proved that the active ingredient for cell penetration remained on the nanoparticle, rather than separated from the liposome, after PLA2 reacted with POPS. Therefore, the final active delivery system was considered to be the enzyme-catalyzed POPS liposomes.

The factors influencing the delivery of POPS-PLA2 were also investigated. The penetration process was tested with different temperatures and inhibitors in stages (Fig. 5L−P). PLA2 still catalyzed the POPS nanoparticles even when the enzyme activity was inhibited by a low temperature of 4 °C (Fig. 5L), which was consistent with the releasing results (Fig. 1G). However, when the cell was treated at 4 °C (Fig. 5M and N) or the enzyme was inhibited by the suitable inhibitor ACA (Fig. 5O), the red PI fluorescence is hardly observed. The specificity of the PLA2 inhibitor was been proved again using the PI staining signal from the inhibitor varespladib-treated group (Fig. 5P), which was similar to the results in Fig. 5B and C. These results demonstrated that both the cell endocytosis and enzyme activity determined the efficacy of drug delivery; specifically, the influence of temperature on endocytosis was stronger than that of the PLA2 enzyme activity.

The dose-effect relationship of each component was also evaluated. At the cellular level, the increase in POPS enhanced cell permeability, indicated by an increase in PI red fluorescence (Fig. 6A); however, this change was not very strong, leading to a small amount of cell damage. However, cell penetration was enhanced sharply with an increase in PLA2 dose (Fig. 6B), leading to more liposome penetration through the cell barrier layer into the lower chamber (Fig. 6C) also as proved in the Transwell system. Additionally, Transwell analysis of the PLA2 enzyme (Fig. 6C) showed no obvious dose-dependent relationship with the permeability of nanoparticles into the barrier layer, but the POPS-PLA2 effect occurred after 10 min. However, *in vivo*, an optimal dose of PLA2 (2.5 U) was established for improving efficacy regarding this targeting effect (Fig. 6D), which differed with the Transwell assay results. Overall, the PLA2 enzyme activity and dosage have a crucial influence on drug penetration into cells.

Finally, the active compounds from the POPS were determined in this study. PLA2 could break the *sn*-2 bond of a phospholipid (Fig. 6E) to produce a corresponding lysophospholipid (Lyso-PL) and fatty acids (FAs), such as oleic acid. Each component was measured using PI staining. The FAs, including oleic acid and palmitic acid, could not affect the permeability of the cell membrane (Fig. 6F). In contrast, lysophosphatidylcholine (LPC) and lysophosphoethanolamine (LPE), the products from phosphatidylcholine (PC) and phosphoethanolamine (PE), could slightly open the cell membrane, leading to PI staining of the nucleus when the concentrations were high, at 100 and 500 μg/mL, respectively (Fig. 6G). Lysophosphatidyl serine (LPHS) had the greatest impact on membrane permeability. T type 16:0 LPHS resulted in a PI-stained nucleus even with a dosage of 20 μg/mL; however, many cells underwent apoptosis following treatment with 200 μg/mL of LPHS. Contrastingly, type 18:1 LPHS had only a small effect when the concentration reached 500 μg/mL (Fig. 6H). Further data have demonstrated that PLA2 had the strongest binding force with PS lipid (POPS, DMPS, DPPS), followed by PC then PE (Fig. 6I and J). These two series experiments established why DPPC and other materials did not work as BTDS despite these compounds having the potential to produce effective cell penetration lyso-material. These results also revealed why POPS had the strongest efficacy in targeting the brain.

The relationship between POPS and PLA2 was further investigated *in vivo*. PLA2 was labeled with fluorescent dyes FITC or Cy7 for effective monitoring and measurement. First, no significant green fluorescence form PLA2-FITC in the brain pathology was observed in Fig. 7A, indicating that PLA2 didn't locate or penetrate into the brain. And then the organs of live fluorescence images (Fig. 7B and C) of animals injected with PLA2-Cy7 and POPS-Cy7, respectively, reflected that the PLA2 didn't bind with POPS liposome and circulated together. The POPS liposome tended to accumulate in the lungs, while proteins of PLA2 tended to accumulate in the livers. In the blood, the content of PLA2-Cy7 gradually decreases after reaching its peak within an hour, whereas that of POPS continues to decrease during the whole monitoring period (Fig. 7D). Finally, administering a mixture of POPS and PLA2 simultaneously, or administering POPS and PLA2 in different orders, did not show any significant differences in the amount of substance transported into the brain as revealed in Fig. 7E. All of evaluations *in vivo* reflected that liposomes (POPS)

presented as mean ± SD ($n = 3$). (D) The FI of dye delivered into the brain of mice treated with POPS combined with different concentrations of PLA2. Data are presented as mean ± SD ($n = 8$). (E) Schematic illustration of phospholipids (PL) converted into lysophospholipids and fatty acids by PLA2 catalytic decomposition. (F, G) Fluorescent images of PI staining of (F) fatty acids and (G) lysophospholipids. (H) Concentration analysis of PI-stained image data for different lysophospholipids. Scale bar = 200 μm. (I, J) Wavelength shift during the binding and dissociation of PL with PLA2. (I) Association and dissociation steps were divided by the dotted line. (J) The binding ratio of PL with PLA2. Data are presented as mean ± SD ($n = 3$). $^{**}P < 0.01$; $^{****}P < 0.0001$ *vs.* indicated. n.s., not significant.

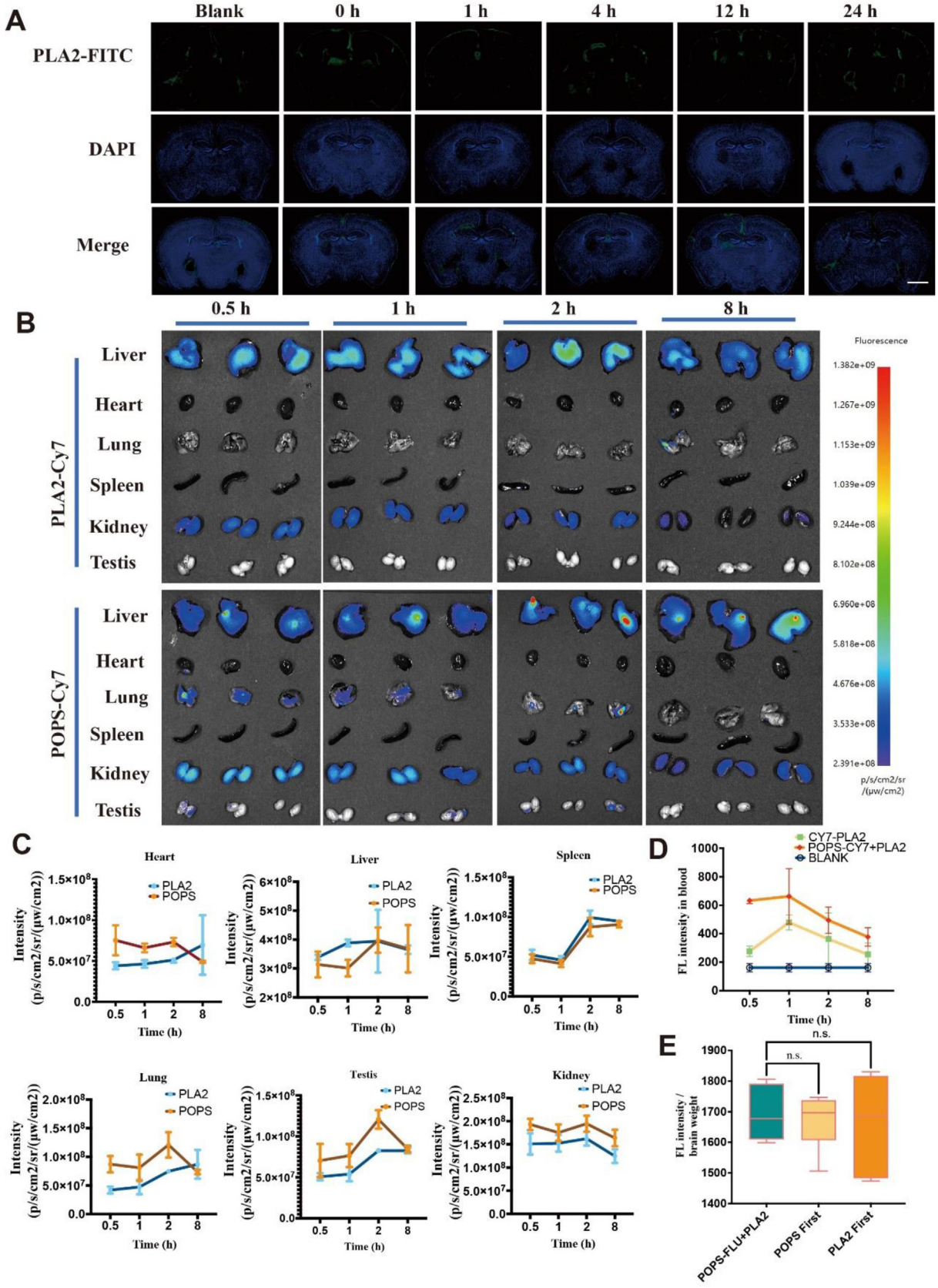

Figure 7 The relationship between POPS and PLA2 *in vivo*. (A) The brain fluorescence pathology of mice administrated with PLA2-FITC during 24 h. Scale bar = 200 μm. (B,C) The main live organs of live fluorescence images (B) and corresponding fluorescence intensity (C) of animals injected with PLA2-Cy7 and POPS-Cy7. (D) The fluorescence intensity in blood. (E) The fluorescence intensity (FI) of dye FLU delivered into the brain of mice treated with different administration orders. Data are presented as mean ± SD (n = 3) (n.s., not significant).

and proteins (PLA2) circulate and metabolize independently in the body, and the order of administration of the two components didn't significantly affect the overall brain target effect.

Other PS materials were investigated to verify the prior findings. The brain targeting effect of DMPS and DPPS combined with PLA2 was measured from cell to mice. All PS could transport drugs into the brain with the help of PLA2 (Fig. 8A), leading to strong brain detoxification against organophosphorus (Fig. 8B). In PI staining, DMPS showed successful nucleus staining when combined with PLA2 (Fig. 8C). Owing to the high PIT and relatively rigid rod molecular structure of DPPS, this material was hard to prepare for liposomes, leading to poor dispersion and formation of a film that covered the cells (Fig. 8D); DPPS was also prone to agglomerate, forming a flocculent precipitate (Fig. 8E). After a week of storage, DMPS liposomes formed a stable gel and were unable to disperse (Fig. 8F). Next, the lethal dosage evaluation was conducted. When the intravenous dose reached 80 mg/kg, all animals in the DMPS group died, whereas all animals in POPS group survived (Fig. 8G). Overall, these results revealed that different types of PS could carry drugs across the BBB with the help of catalysis of PLA2; nonetheless, POPS was the best candidate for the BTDS owing to its relatively higher safety than DMPS and easier preparation than DPPS.

3.6. *BTDS safety*

PLA2 is an early biomarker and accelerator for inflammation[42,43]; the application of PLA2 must be within a safe and reliable dose range. Treatment with PLA2, POPS and all the opening materials alone were determined to be safe, as indicated by Cell proliferation and toxicity analysis (Fig. 9A and B, Supporting Information Fig. S7) and pathology of main organs (Supporting Information Fig. S8). Although POPS-PLA2 influenced integrity, no apoptosis occurred following treatment with POPS (800 mg/mL) combined with PLA2 below 0.0156 U/mL or PLA2 (0.1 U/mL) combined with POPS below 0.2 mg/mL (Fig. 9C). Beside cytotoxicity, the evaluation of erythrocyte hemolysis *in vitro* reflected the same process (Fig. 9D and E). POPS combined with the PLA2 caused hemolysis only if the treatment concentration was above 0.024 mg/mL POPS and 0.3 U/mL PLA2 (Fig. 9E). All of the individual components, including the reactivator HI-6, were considered to be safe for cells (Fig. 9E). In animal models determined *via* blood biochemistry (Fig. 8F–H), only aspartate aminotransferase (AST) levels were abnormal when rats were treated with a high dosage of PLA2 (50 U) with POPS (Fig. 9G). The corresponding pathology results confirmed that no damage was observed in the main organs when the combination of POPS and PLA2 was used at a safe concentration (POPS 8 mg/mL, PLA2 50 U/mL; Fig. 9I and Supporting Information Fig. S9).

Evaluating the lethality of each component in mice showed that PLA2 and POPS alone did not cause animal death at 25–400 U/mL and 2–16 mg/mL, respectively (Fig. 9J). When the two components were mixed, the mixture would cause death at concentrations greater than 8 mg/mL for POPS and 200 U/mL for PLA2. When treated with PLA2 alone under 1000 U, the rat was considered to be safe, with the BBB maintaining its barrier function, which inhibited the transport of molecules into the brain.

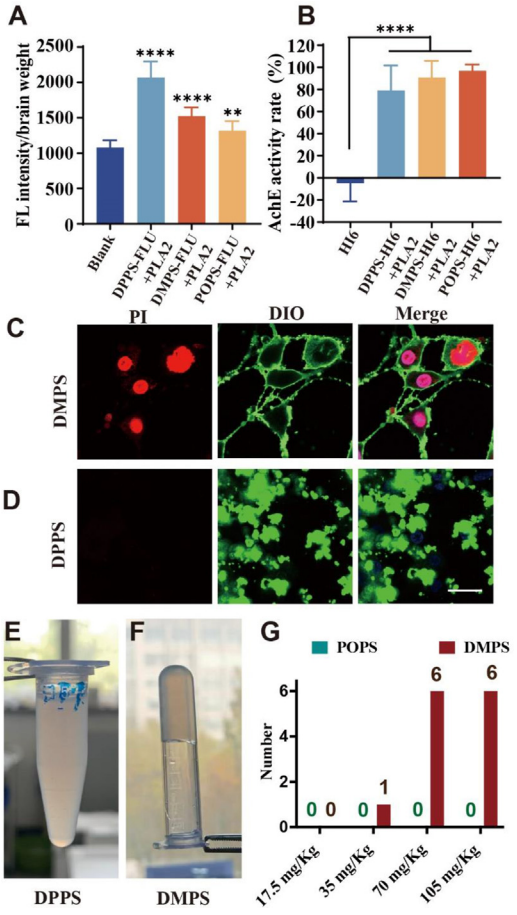

Figure 8 The brain targeting effect and biocompatibility of other PS materials. (A) The FI of dye delivered into the brain of mice treated with different PS combined with PLA2. Data are presented as mean ± SD ($n = 8$). (B) The brain ARR when treated with different PS combined with PLA2. Data are presented as mean ± SD ($n = 8$) (**$P < 0.01$; ****$P < 0.0001$ *vs.* indicated). (C and D) Fluorescent images of PI staining with (C) DMPS and (D) DPPS. Scale bar = 50 μm. (E and F) Images of a suspension of DPPS and hydrogel of DMPS. (G) The number of animal deaths following administration with POPS or DMPS at various doses ($n = 6$).

Beyond the safe dosage of PLA2, the animal would die, due to a dysfunctional BBB and large amounts of molecules penetrating the brain (Fig. 9K). In the studied drug delivery system, the concentrations of the two components we used were determined to be within the safe range.

The persistence and restorability of POPS-PLA2 were also key for BTDS safety. Cells stained with PI were used to determine the recovery time after POPS-PLA2 treatment (Fig. 9L). Then, 2 h after stimulation from POPS-PLA2, PI could no longer penetrate the cell membrane to stain the nucleus due to the recovery of membrane integrity (Fig. 9M) and the molecules couldn't penetrate through the bEnd.3 cell layer in BBB Transwell system totally after 24 h (Supporting Information Fig. S10). The following results demonstrated that combining POPS with PLA2 was safe in the concentration we used for brain target delivery;

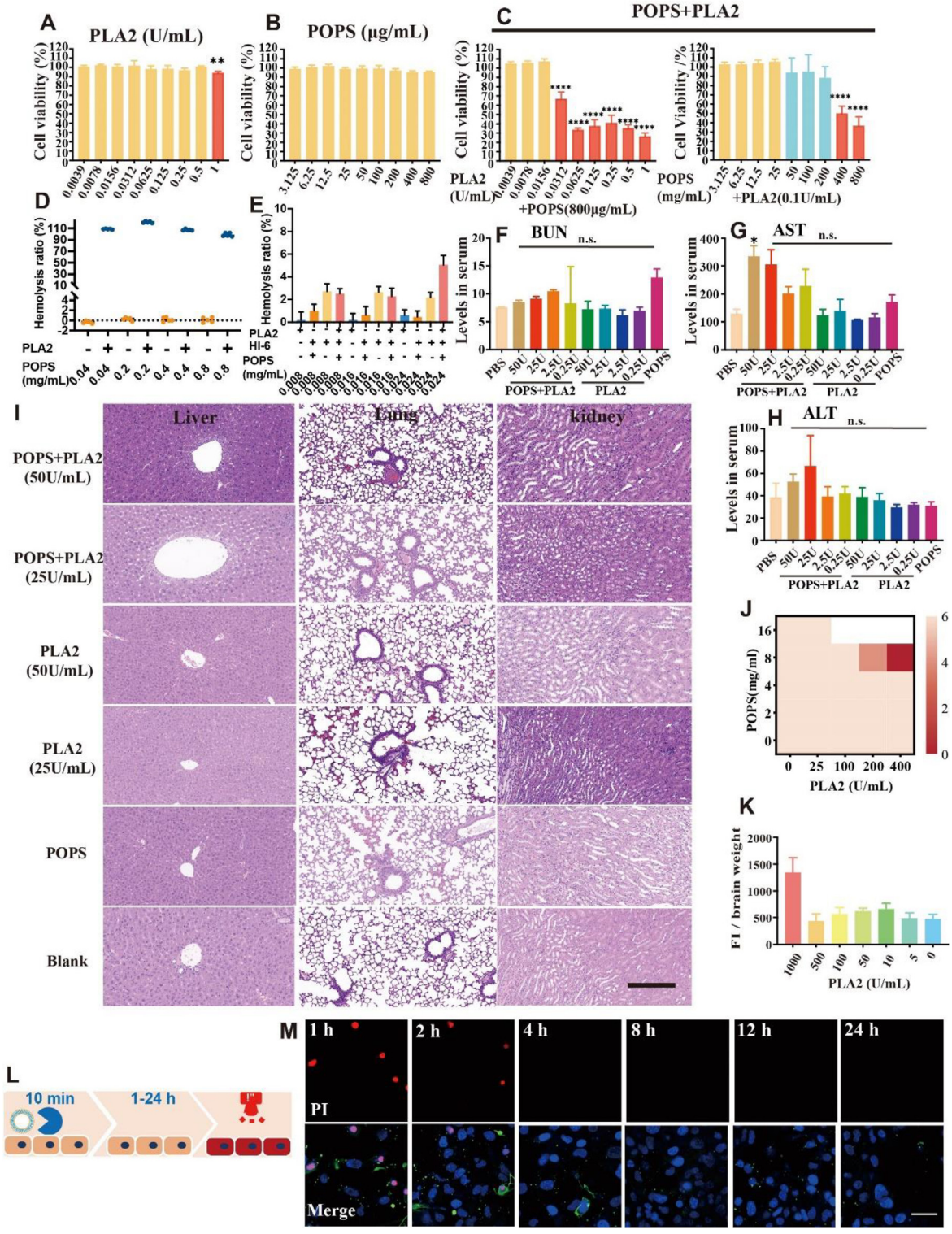

Figure 9 The safety evaluation of POPS and PLA2. (A−C) Viability of bEnd. 3 cells treated with (A) PLA2 alone, (B) POPS alone, or (C) POPS combined with PLA2. Data are presented as mean ± SD (n = 6). (D and E) Erythrocytic hemolysis of cells treated with (D) PLA2 (0.125−2.5 U/mL), POPS (0.04−0.8 mg/mL), (E) PLA2 (0.025−0.075 U/mL), POPS (0.008−0.024 mg/mL), or HI-6 (0.003−0.009 mg/mL). Data are presented as mean ± SD (n = 3). (F−H) Blood biochemistry of (F) blood urea nitrogen (BUN), (G) AST, (H) alanine transaminase (ALT) in mice treated with POPS combined with PLA2. Data are presented as mean ± SD (n = 3). (I) Images of H&E-stained liver, lung, and kidney sections. Scale bar = 200 μm. (J) Lethality of POPS, PLA2, and POPS combined with PLA2 at various concentrations (n = 6). (K) The FI of dye delivered into the brain of mice treated with PLA2 at various concentrations. Data are presented as mean ± SD (n = 8). (L) Schematic diagram evaluating the recovery time after POPS combined with PLA2 after interacting with cells for 10 min and (M) corresponding fluorescent images of PI staining (n.s., not significant). Scale bar = 50 μm.

additionally, the BBB opening process activated by this combination was reversible.

4. Conclusions

In this study, the strategy of selectively opening the BBB was proposed with the construction of a BTDS, using an ultra-simple structure and components. Based on the screening of BBB opening and matrix delivery materials, the strongest candidate was the combination of POPS liposomes and PLA2, which effectively transport molecules into the brain. The mechanism responsible for this was identified, showing that the enzyme PLA2 catalyzed the POPS liposome into LPS nanoparticles immediately, which allowed for efficient delivery of drugs into the brain. During this process, the BBB consistently exhibited a comprehensive inhibitory effect against all molecules, permitting only the passage of LPS nanoparticles into the brain. The utilization of POPS and PLA2 in combination was found to be both safe and effective at a specific dosage., and cells treated with these two materials displayed prompt restoration. Most PS observed in this study capable of effectively transporting drugs across the BBB into the brain when combined with PLA2. This demonstrated a significant advantage over other liposome materials, such as PC and PE. Specifically, POPS was the optimum PS material owing to its high safety and stable preparation. By utilizing this BTDS, a novel brain-targeted nano-antidote was efficiently prepared. This BTDS possessed the most effective detoxification effect against organophosphorus poisoning, surpassing any previously observed effects. Further, the BTDS created using this strategy exhibited an ultra-simple structure and can be efficiently manufactured in large quantities while maintaining strict quality standards. In brief, the combination of POPS and PLA2 presents a highly encouraging therapeutic delivery system for addressing central nervous system disorders.

Acknowledgments

This work was supported by the Equipment comprehensive research Project, the Zhi Qiang Innovation Project. The data that support the findings of this study are available from the corresponding author upon reasonable request.

Author contributions

Zinan Zhang and Wenbin Cao contributed equally to this work. Zinan Zhang, Wenbin Cao: Conceptualization, Methodology, Investigation, Writing−Original Draft. Huanchun Xing, Shuai Guo: Methodology, Formal Analysis, Data Curation. Lijuan Huang, Lin Wang: Data Curation, Validation. Sui Xin, Kui Lu, Yuan Luo: Supervision, Validation, Funding Acquisition. Yongan Wang, Jun Yang: Conceptualization, Funding Acquisition, Resources, Supervision, Writing−Review & Editing.

Conflicts of interest

The authors declare no conflicts of interest.

Appendix A. Supporting information

Supporting data to this article can be found online at https://doi.org/10.1016/j.apsb.2023.11.015.

References

1. Levin VA, Tonge PJ, Gallo JM, Birtwistle MR, Dar AC, Iavarone A, et al. CNS anticancer drug discovery and development conference white paper. *Neuro Oncol* 2015;**17**(Suppl 6):vi1−26.
2. Nussbaum RL, Ellis CE. Alzheimer's disease and Parkinson's disease. *N Engl J Med* 2003;**348**:1356−64.
3. Zhao YF, Zhang XJ, Chen XY, Wei Y. Neuronal injuries in cerebral infarction and ischemic stroke: from mechanisms to treatment. *Int J Mol Med* 2022;**49**:1−9.
4. Fu HY, Tan P, Wang RJ, Li SL, Liu HZ, Yang Y, et al. Advances in organophosphorus pesticides pollution: current status and challenges in ecotoxicological, sustainable agriculture, and degradation strategies. *J Hazard Mater* 2022;**424**:127494.
5. Nance E, Pun SH, Saigal R, Sellers DL. Drug delivery to the central nervous system. *Nat Rev Mater* 2022;**7**:314−31.
6. Sethi B, Kumar V, Mahato K, Coulter DW, Mahato RI. Recent advances in drug delivery and targeting to the brain. *J Control Release* 2022;**350**:668−87.
7. Bashyal S, Thapa C, Lee S. Recent progresses in exosome-based systems for targeted drug delivery to the brain. *J Control Release* 2022;**348**:723−44.
8. You LH, Wang J, Liu TQ, Zhang YL, Han XX, Wang T, et al. Targeted brain delivery of rabies virus glycoprotein 29-modified deferoxamine-loaded nanoparticles reverses functional deficits in parkinsonian mice. *ACS Nano* 2018;**12**:4123−39.
9. Song Y, Du D, Li L, Xu J, Dutta P, Lin YH. *In vitro* study of receptor-mediated silica nanoparticles delivery across blood-brain barrier. *ACS Appl Mater Interfaces* 2017;**9**:20410−6.
10. Zhang YD, He JL, Shen L, Wang T, Yang J, Li Y, et al. Brain-targeted delivery of obidoxime, using aptamer-modified liposomes, for detoxification of organophosphorus compounds. *J Control Release* 2021;**329**:1117−28.
11. Terstappen GC, Meyer AH, Bell RD, Zhang W. Strategies for delivering therapeutics across the blood-brain barrier. *Nat Rev Drug Discov* 2021;**20**:362−83.
12. Dong X. Current strategies for brain drug delivery. *Theranostics* 2018;**8**:1481−93.
13. Sheikov N, McDannold N, Sharma S, Hynynen K. Effect of focused ultrasound applied with an ultrasound contrast agent on the tight junctional integrity of the brain microvascular endothelium. *Ultrasound Med Biol* 2008;**34**:1093−104.
14. Zhang JL, Liu H, Du XS, Guo Y, Chen X, Wang SN, et al. Increasing of blood-brain tumor barrier permeability through transcellular and paracellular pathways by microbubble-enhanced diagnostic ultrasound in a c6 glioma model. *Front Neurosci* 2017;**11**:86.
15. Bennewitz MF, Saltzman WM. Nanotechnology for delivery of drugs to the brain for epilepsy. *Neurotherapeutics* 2009;**6**:323−36.
16. Siegal T, Rubinstein R, Bokstein F, Schwartz A, Lossos A, Shalom E, et al. *In vivo* assessment of the window of barrier opening after osmotic blood−brain barrier disruption in humans. *J Neurosurg* 2000;**92**:599−605.
17. Ramachandran S, Satapathy SR, Dutta T. Delivery strategies for mRNA vaccines. *Pharmaceut Med* 2022;**36**:11−20.
18. Eygeris Y, Gupta M, Kim J, Sahay G. Chemistry of lipid nanoparticles for RNA delivery. *Acc Chem Res* 2022;**55**:2−12.
19. Vieira DB, Gamarra LF. Getting into the brain: liposome-based strategies for effective drug delivery across the blood−brain barrier. *Int J Nanomed* 2016;**11**:5381.
20. Shaw TK, Paul P. Recent approaches and success of liposome-based nano drug carriers for the treatment of brain tumor. *Curr Drug Deliv* 2022;**19**:815−29.
21. Murakami M, Kudo I. Phospholipase A2. *J Biochem* 2002;**131**:285−92.
22. Yang J, Fan LX, Wang FJ, Luo Y, Sui X, Li WH, et al. Rapid-releasing of HI-6 *via* brain-targeted mesoporous silica nanoparticles for nerve agent detoxification. *Nanoscale* 2016;**8**:9537−47.
23. Perriere N, Demeuse P, Garcia E, Regina A, Debray M, Andreux JP, et al. Puromycin-based purification of rat brain capillary endothelial

cell cultures. Effect on the expression of blood−brain barrier-specific properties. *J Neurochem* 2005;**93**:279−89.
24. Li Y, Huang LJ, Zhang ZN, Huang JY, Xing HC, Wang L, et al. An *in vitro* nerve agent brain poisoning transwell model for convenient and accurate antidote evaluation. *Toxicol in Vitro* 2023;**88**:105541.
25. Banks WA, Gray AM, Erickson MA, Salameh TS, Damodarasamy M, Sheibani N, et al. Lipopolysaccharide-induced blood-brain barrier disr uption: roles of cyclooxygenase, oxidative stress, neuroinflammation, and elements of the neurovascular unit. *J Neuroinflammation* 2015;**12**:223.
26. Lundy DJ, Lee KJ, Peng IC, Hsu CH, Lin JH, Chen KH, et al. Inducing a transient increase in blood−brain barrier permeability for improved liposomal drug therapy of glioblastoma multiforme. *ACS Nano* 2019;**13**:97−113.
27. Kim DG, Bynoe MS. A2A adenosine receptor modulates drug efflux transporter P-glycoprotein at the blood−brain barrier. *J Clin Invest* 2016;**126**:1717−33.
28. Chu CY, Jablonska A, Lesniak WG, Thomas AM, Lan XY, Linville RM, et al. Optimization of osmotic blood−brain barrier opening to enable intravital microscopy studies on drug delivery in mouse cortex. *J Control Release* 2020;**317**:312−21.
29. Wu T, Zhang AQ, Lu HY, Cheng QY. The role and mechanism of borneol to open the blood−brain barrier. *Integr Cancer Ther* 2018;**17**: 806−12.
30. Sui YT, Chen Y, Lv QY, Zheng YL, Kong DC, Jiang H, et al. Suilyin disrupts the blood−brain barrier by activating group III secretory phospholipase A2. *Life (Basel)* 2022;**12**:919.
31. Hartz AMS, Rempe RG, Soldner ELB, Pekcec A, Schlichtiger J, Kryscio R, et al. Cytosolic phospholipase A2 is a key regulator of blood-brain barrier function in epilepsy. *FASEB J* 2019;**33**:14281−95.
32. Nito C, Kamada H, Endo H, Niizuma K, Myer DJ, Chan PH. Role of the p38 mitogen-activated protein kinase/cytosolic phospholipase A2 signaling pathway in blood−brain barrier disruption after focal cerebral ischemia and reperfusion. *J Cereb Blood Flow Metab* 2008;**28**: 1686−96.
33. Han L, Jiang C. Evolution of blood−brain barrier in brain diseases and related systemic nanoscale brain-targeting drug delivery strategies. *Acta Pharm Sin B* 2021;**11**:2306−25.
34. Esquerda-Canals G, Montoliu-Gaya L, Güell-Bosch J, Villegas S. Mouse models of Alzheimer's disease. *J Alzheimers Dis* 2017;**57**:1171−83.
35. Niu WB, Xiao Q, Wang XJ, Zhu JQ, Li JH, Liang XM, et al. A Biomimetic drug delivery system by integrating grapefruit extracellular vesicles and doxorubicin-loaded heparin-based nanoparticles for glioma therapy. *Nano Lett* 2021;**21**:1484−92.
36. Lundy PM, Hamilton MG, Sawyer TW, Mikler J. Comparative protective effects of HI-6 and MMB-4 against organophosphorous nerve agent poisoning. *Toxicology* 2011;**285**:90−6.
37. Musilek K, Korabecny J, Jun D, Kassa J, Kuca K. Novel cholinesterase reactivators. In: Gupta Ramesh C, editor. *Handbook of toxicology of chemical warfare agents*. Amsterdam: Elsevier; 2015. p. 1071−87.
38. Shih TM, Skovira JW, O'Donnell JC, McDonough JH. *In vivo* reactivation by oximes of inhibited blood, brain and peripheral tissue cholinesterase activity following exposure to nerve agents in Guinea pigs. *Chem Biol Interact* 2010;**187**:207−14.
39. Chowdhary S, Bhattacharyya R, Banerjee D. Acute organophosphorus poisoning. *Clin Chim Acta* 2014;**431**:66−76.
40. Aron M, Vince O, Gray M, Mannaris C, Stride E. Investigating the role of lipid transfer in microbubble-mediated drug delivery. *Langmuir* 2019;**35**:13205−15.
41. Youngman NJ, Walker A, Naude A, Coster K, Sundman E, Fry BG. Varespladib (LY315920) neutralises phospholipase A2 mediated prothrombinase-inhibition induced by Bitis snake venoms. *Comp Biochem Physiol C Toxicol Pharmacol* 2020;**236**:108818.
42. Peng ZX, Chang YX, Fan JH, Ji WD, Su CQ. Phospholipase A2 superfamily in cancer. *Cancer Lett* 2021;**497**:165−77.
43. Murakami M, Nakatani Y, Atsumi GI, Inoue K, Kudo I. Regulatory functions of phospholipase A2. *Crit Rev Immunol* 2017;**37**: 127−95.